Measurement-based Analysis of XL-MIMO Channel Characteristics in a Corridor Scenario

Qi Wei[1], Pan Tang[1], Haiyang Miao[1], Weirang Zuo[1], Lei Tian[1], Jianhua Zhang[1], Guangyi Liu[2], and Mengnan Jian[3,4]
[1]State Key Lab of Networking and Switching Technology,
Beijing University of Posts and Telecommunications, Beijing 100876, China;
{weiqi0814, tangpan27, hymiao, zuoweirang, tianlbupt, jhzhang}@bupt.edu.cn.
[2]China Mobile Research Institute, Beijing 100053, China;
liuguangyi@chinamobile.com.
[3]State Key Laboratory of Mobile Network and Mobile Multimedia Technology, Shenzhen 518055, China;
[4]Wireless Research Institute, ZTE Corporation, Beijing 100029, China;
jian.mengnan@zte.com.cn

2024 IEEE 99th Vehicular Technology Conference (VTC2024-Spring) | 979-8-3503-8741-4/24/$31.00 ©2024 IEEE | DOI: 10.1109/VTC2024-SPRING62846.2024.10683481

***Abstract*—Extremely large-scale massive multiple-input multiple-output (XL-MIMO) is a potential enabling technology for 6th-generation (6G) communication. The XL-MIMO channel research will be important for XL-MIMO system development. In this paper, the measurement of XL-MIMO channels from 32 to 512 transmitting antenna elements in the 6 GHz band is carried out in an indoor corridor scenario. The delay spread, angular spread, and channel capacity are investigated. The results are compared with the indoor channel model in the Third Generation Partnership Project (3GPP) TR 38.901. We find that the number of antenna elements has a small impact on the delay spread and angular spread. So the spatial non-stationary effect does not need to be considered specifically in the far-field range in this scenario. In addition, the special structure of the corridor leads to a difference in the comparison of the angular spread with the 3GPP model in each dimension. The closed environment of the corridor also results in a significant gap in channel capacity performance from the i.i.d. channel. This work can provide insights into XL-MIMO applications in the 6G era.**

***Index Terms*—XL-MIMO, channel measurements, 6 GHz, 6G, 3GPP**

I. Introduction

With the large-scale application of 5th-generation (5G) communication systems, countries, and organizations worldwide are actively conducting research related to next-generation communication systems [1]-[3]. To cope with the further growth of data traffic, extremely large-scale massive multiple-input multiple-output (XL-MIMO) is considered one of the key technologies to address the growth of data traffic [1]. XL-MIMO is a further evolution of massive MIMO. According to the theoretical analysis [4], with the gradual increase in the number of antenna units deployed on the base station, the channel between different antenna elements tends to be orthogonal, which significantly improves the security, energy efficiency, spatial efficiency, and robustness of the XL-MIMO system. XL-MIMO is a powerful technology to support high-traffic scenarios. In the 5G and 6G era, more than 80% of data traffic will be generated indoors [5], making indoor scenarios one of the potential scenarios for deploying XL-MIMO.

The research on XL-MIMO channel characterization is important for the development of XL-MIMO systems. So far, a series of measurement-based channel characterization and modeling of XL-MIMO has been performed. In [6], outdoor channel measurements at 2.6 GHz are performed with two types of XL-MIMO arrays. In [7], the outdoor-to-indoor (O2I) delay spread characteristics of XL-MIMO systems at 3.5 GHz are analyzed. In [8], the evolution of cluster number based on 256 virtual arrays was given in the 3.5 GHz band under line-of-sight (LOS) and non-line-of-sight (NLOS) conditions respectively. Most of the current research on XL-MIMO is in open outdoor environments. How it performs in relatively closed indoor environments is yet to be investigated.

In addition, to solve the problem of existing spectrum resource constraints, the new mid-band spectrum (6-24 GHz) has attracted a great deal of attention from both academia and industry [9] [10]. In June 2022, 3GPP formally defined the U6G (the upper half of 6 GHz, i.e., 6425-7125 MHz) authorized spectrum. This conference resulted in 5G-Advanced Rel-18 project approval for the full 6 GHz spectrum (5925 MHz-7125 MHz), which is a key milestone in the IMT-ization of the 6 GHz spectrum. Qualcomm and Samsung also released 6G white papers explaining their considerations for the 6G spectrum [11] [12]. China Mobile has a 6 GHz spectrum under consideration for 5G-Advanced and 6G [13]. In the World Radiocommunication Conference 2023 (WRC-23) in December 2023, it was proposed to identify the 6 GHz spectrum for mobile in every ITU Region [14]. Therefore 6 GHz is a frequency of great interest and it is essential to research the channel characteristics at 6 GHz. Measurement and analysis in [15] demonstrate the superiority of 6 GHz in communications.

In this paper, we perform an XL-MIMO channel measurement with transmitting antenna elements from 32 to 512 and analyze the impact of the number of antennas and the environment on the channel characteristics. The contributions of this paper are summarized as follows:

- The XL-MIMO channel measurement with the number

of transmitting antennas from 32 to 512 is performed in a corridor scenario using a measurement system with a high-speed electronic switching matrix based on time-division multiplexing (TDM)-MIMO.
- By processing the measurement data, the power delay profile (PDP), delay spread, angular spread, and channel capacity are obtained. The impact of the number of antennas on channel characteristics and capacity is analyzed.
- The delay spread and angular spread are compared with the indoor channel model parameters in 3GPP TR 38.901. The impact of the environment on channel characteristics and capacity is analyzed.

The rest of the paper is organized as follows: In section II, the measurement platform, scenario, and data processing method are described. Section III shows the results and analysis of the channel characteristics. Section IV concludes this paper.

II. Measurements and Data Processing

A. Measurement System

In this paper, the measurement platform used is based on the principle of time domain spread spectrum sliding correlation. The high-speed electronic switching switch can complete XL-MIMO channel measurement within one hundred milliseconds, making it a reality to measure the comprehensive characteristics of medium and low-frequency MIMO channels based on TDM-MIMO mode. Combined with pseudo-random (PN) sequence signal and time division multiplexing antenna switching technology, it can decouple the response of the measurement system itself.

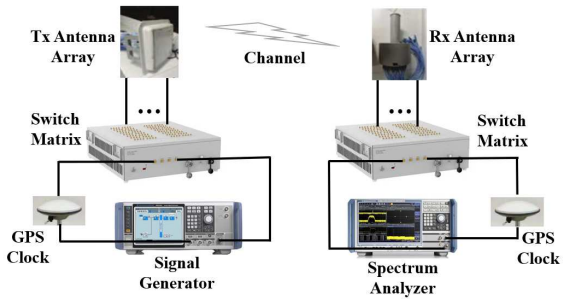

Fig. 1. Schematic diagram of massive MIMO channel measurement platform.

Fig. 1 shows the simplified structure diagram of the measurement platform. The transmitter consists of a high-frequency signal generator, a control computer, a switching matrix, a GPS clock module, RF lines, and a 32-element uniform planar antenna array (UPA). The receiver comprises a 56-element omnidirectional antenna array (ODA), RF lines, a spectrum analyzer, a control computer, a switching matrix, and a GPS clock module. The transceiver antenna matrix module uses the reference clock provided by the GPS module to achieve high-precision synchronization start and synchronization unit switching. The signal transceiver uses the 10 MHz reference clock provided by the GPS module to ensure the consistency of the baseband signal at the transmitter side, the signal carrier frequency and I/Q demodulation frequency at the receiver side, and the time domain sampling time sequence. High synchronization accuracy of signal transmission, antenna switching, and signal acquisition is achieved. Table. I shows more parameter configurations for the measurement system.

TABLE I
MEASUREMENT SYSTEM CONFIGURATION

Parameter	Configuration
Center frequency [GHz]	6
Chip length	511
Symbol rate [MBaud]	50
Bandwidth [MHz]	100
Antenna type	Tx: UPA /Rx: ODA
Element number	Tx: 32/Rx: 56
Tx/Rx height [m]	Tx: 1.7/Rx: 1.5

During the measurement, a virtual XL-MIMO array with a maximum of 512 antenna elements is composed by moving the UPA horizontally and vertically, as shown in Fig. 2. The spacing between array elements is $\lambda/2$, and the overall size of XL-MIMO is 0.8 m$\times$0.2 m. The rationality of this virtual XL-MIMO measurement method from the point of spatial propagation properties is given in [16].

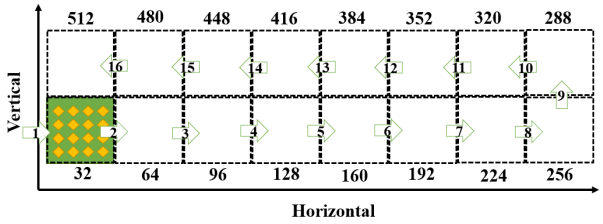

Fig. 2. Principal diagram of XL-MIMO array.

B. Measurement Scenario

The measurement scenario is in the Beijing University of Posts and Telecommunications (BUPT), China. The corridor is divided into two segments perpendicular to each other, which represents the LoS and NLoS cases. As shown in Fig. 3, Tx is placed at the south end of the corridor, and Rx takes 7 points in each case. The Rayleigh distance $R=2D^2/\lambda$ is calculated as 27.2 m, where D is taken as the hypotenuse of the XL-array. The first measuring point is 30 m away from the transmitter, so the transmitting and receiving ends were always outside the near-field range of the antenna array. Therefore, the spherical wavefront was not considered. The reason for choosing to measure here is that the corridor is a special scenario, and its narrow structure causes the channel characteristics to be different from Indoor Hotspot (InH)-Office scenarios.

The measurement campaign takes place at night when no one is around to ensure that the channel is time quasi-

(a)

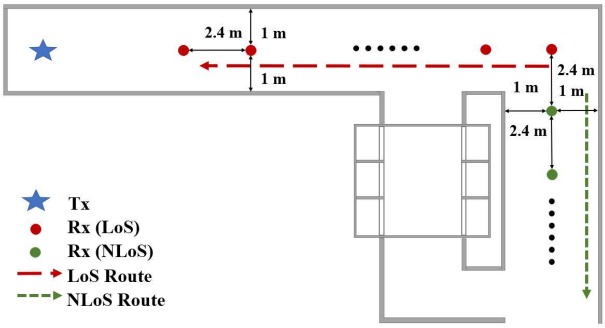

(b)

Fig. 3. Channel measurement in the corridor scenario. (a) Transceiver antenna location. (b) Layout of measurement scenario.

stationary when the UPA is shifted within one sampling cycle.

C. Data Processing

1) CIR: To obtain the pure channel impulse response (CIR), removing the impact of the measurement system with a back-to-back calibration is necessary. Based on the channel measurement platform used, the received signal in the delay domain can be expressed as

$$y_{mea}(\tau) = x(\tau) * h^{tx}(\tau) * G^{tx}(\tau) * h(\tau) * G^{rx}(\tau) * h^{rx}(\tau), \quad (1)$$

where "$*$" is convolution in the time domain, x denotes the transmitted signal, and y_{data} is the received signal. h^{tx}, G^{tx}, h, G^{rx} and h^{rx} denote the transfer function of the transmitter system, the transmitter antenna, the channel, the receiver antenna, and the receiver system, respectively. Its frequency domain representation can be obtained from the Fourier transform as

$$y_{mea}(f) = x(f) \cdot h^{tx}(f) \cdot G^{tx}(f) \cdot h(f) \cdot G^{rx}(f) \cdot h^{rx}(f), \quad (2)$$

The calibration signal in the frequency domain can be expressed as

$$y_{cal}(f) = x(f) \cdot h^{tx}(f) \cdot h^{rx}(f), \quad (3)$$

the antenna response G^{tx} and G^{rx} can be obtained by measuring in an anechoic chamber. Assuming that the system is linear, the CIR can be calculated as

$$h(\tau) = IFFT\left(\frac{y_{mea}(f)}{y_{cal}(f) \cdot G^{tx} \cdot G^{rx}}\right), \quad (4)$$

By combining the 16 groups of CIR that were calculated from raw data, the CIR of a 512-element array is obtained. Then the spatial-temporal MPC parameters can be extracted by using the SAGE algorithm.

2) PDP & RMS Delay Spread: The PDP visualizes the delay dispersion of the MPCs, and the power of the MPC l with a delay of τ_l is calculated as:

$$P_l = |h(\tau_l)|^2, l = 1, 2, \ldots, L, \quad (5)$$

where it is assumed that the massive MIMO channel has a total of L MPCs.

Root-mean-square (RMS) delay spread reflects the statistical properties of delay dispersion and is one of the most commonly used parameters in wireless channel research. The RMS delay spread is calculated as

$$\tau_{rms} = \sqrt{\frac{\sum_{l=1}^{L}(\tau_l - \tau_{mean})^2 P_l}{\sum_{l=1}^{L} P_l}}, \quad (6)$$

where τ_{mean} denotes the average excess delay, which is calculated as

$$\tau_{mean} = \frac{\sum_{l=1}^{L} \tau_l P_l}{\sum_{l=1}^{L} P_l}, \quad (7)$$

3) Angular Spread: Angular spread can quantitatively reflect the degree of MPCs diffusion in space. The root mean square angular spread is calculated as follows

$$\psi_{rms} = \sqrt{\frac{\sum_{l=1}^{L}(\psi_l - \psi_{mean})^2 P_l}{\sum_{l=1}^{L} P_l}}, \quad (8)$$

where ψ_l represents the azimuth angle ϕ_l or elevation angle θ_l of the lth MPC, and ψ_{mean} can be calculated as

$$\psi_{mean} = \frac{\sum_{l=1}^{L} \psi_l P_l}{\sum_{l=1}^{L} P_l}, \quad (9)$$

We calculated the RMS angular spread of the azimuth angle of departure, elevation angle of departure, azimuth angle of arrival, and elevation angle of arrival, denoted as ASD, ESD, ASA, and ESA, respectively.

4) Channel Capacity: Channel capacity reflects the maximum amount of information that can be transmitted by the channel. According to [17], the channel capacity can be calculated as:

$$C = \frac{1}{B}\int_B \log_2 det\left(\mathbf{I}_M + \frac{\rho}{N}\mathbf{H}(f)\mathbf{H}^H(f)\right)df, \quad (10)$$

where N is the number of transmitting antenna elements and M is the number of receiving antenna elements. $\mathbf{I}_M$ is an $M \times M$ unit matrix, ρ denotes the transmission signal-to-noise ratio (SNR), B denotes the system bandwidth, and $(\cdot)^H$ is a

Hermitian operation. The mean channel capacity realized can be given by

$$\tilde{C}(\rho) = \frac{1}{K}\sum_{k=1}^{K} \log_2 det\left(\mathbf{I}_M + \frac{\rho}{\beta N}\mathbf{H}_r\mathbf{H}_r^H\right), \tag{11}$$

where K is the number of channel realizations, $\mathbf{H}_r$ is the discrete channel that has been realized and β is a common normalization factor for all $\mathbf{H}_r$ within one snapshot which can be expressed as

$$E\left\{\frac{1}{\beta}\|\mathbf{H}_r\|_F^2\right\} = N \cdot M, \tag{12}$$

that makes the average channel power gain unitarily, $\|\cdot\|_F$ denotes the Frobenius norm.

III. Channel Characteristics Analysis

A. PDP & RMS Delay Spread

Take the LoS environment as an example, we draw the PDP by listing the average power of MPCs and their corresponding excess delays in Fig. 4. The comparison shows that the PDP envelopes of XL-MIMO channels with different numbers of transmitting elements are very similar. This is because the MPCs are relatively fixed in the corridor scenario and spatial non-stationarity does not have a significant effect at far-field distances. This conclusion is also reflected in the RMS delay spread results.

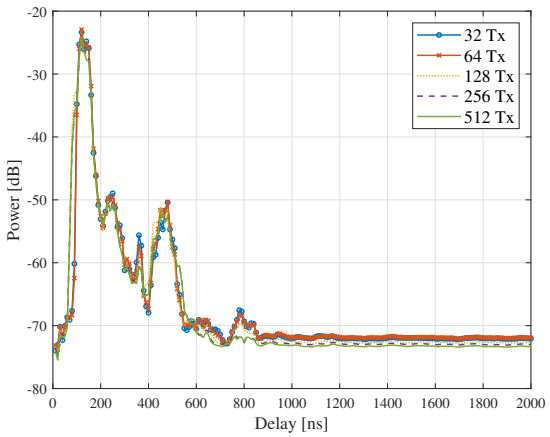

Fig. 4. PDP comparison of various numbers of TX elements in LoS.

Table. II shows the RMS delay spread results. It can be seen that the number of antenna elements has a small effect on the mean value of the delay spread, both in LoS and NLoS. In addition, the measured delay spread is compared with the 3GPP model parameters for indoor scenarios. Such as in Fig. 5 the results in the LoS environment are not much different in the mean value.

So we can conclude that the delay domain parameters do not need to consider the effect of the number of antenna elements in XL-MIMO channel modeling. In addition, under far-field conditions, spatial non-stationarity does not significantly affect the delay domain characteristics.

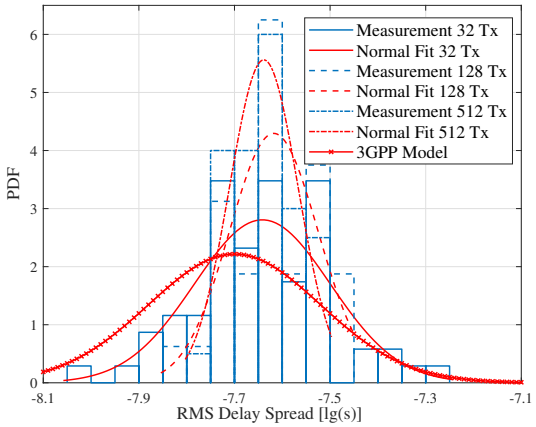

Fig. 5. RMS delay spread comparison of various numbers of TX elements and 3GPP model in LoS.

TABLE II
THE RMS DELAY SPREAD IN CORRIDOR SCENARIO VS. 3GPP

Measurement case	LoS/NLoS	μ $\log_{10}[s]$	σ
32 Tx	LoS	-7.63	0.13
	NLoS	-7.43	0.16
64 Tx	LoS	-7.62	0.15
	NLoS	-7.45	0.10
128 Tx	LoS	-7.65	0.09
	NLoS	-7.43	0.10
256 Tx	LoS	-7.64	0.13
	NLoS	-7.46	0.04
512 Tx	LoS	-7.62	0.07
	NLoS	-7.41	0.04
3GPP InH-Office [18]	LoS	-7.70	0.18
	NLoS	-7.41	0.14

B. RMS Angular Spread

Table. III shows the RMS angular spread results for XL-MIMO with different numbers of antenna elements. It can be seen that there is no significant change in the angular spread as the number of antenna elements increases. The reason for the insignificant change is the structure of the corridor, which results in a relatively fixed angle of MPCs. Measurement in the outdoor scenario in [19], when the antenna increases, the angular spread changes significantly. A comparison of the measured angular spread results with the 3GPP indoor model is also given in Table. III, the comparison results are different for different dimensions. The ASD is smaller than the model parameters because the corridor structure is narrow and long, and the MPCs with large departure angles cannot reach the receiver. The comparison of ASA is special, as shown in Fig. 6. In the LoS environment, the measured results are larger than the model parameters, because the received MPCs mainly consist of the signal propagated from the front and the signal reflected from the end of the corridor. In the

TABLE III
THE RMS ANGULAR SPREAD IN CORRIDOR SCENARIO VS. 3GPP

Measurement Case	LoS/NLoS	ASD ($log_{10}[^\circ]$)		ESD ($log_{10}[^\circ]$)		ASA ($log_{10}[^\circ]$)		ESA ($log_{10}[^\circ]$)	
		μ	σ	μ	σ	μ	σ	μ	σ
32 Tx	LoS	1.33	0.37	1.40	0.14	1.74	0.18	1.54	0.27
	NLoS	1.34	0.37	1.28	0.35	1.75	0.35	1.41	0.40
64 Tx	LoS	1.36	0.42	1.49	0.13	1.70	0.41	1.49	0.31
	NLoS	1.32	0.49	1.42	0.08	1.70	0.38	1.37	0.51
128 Tx	LoS	1.36	0.44	1.48	0.19	1.68	0.25	1.50	0.29
	NLoS	1.49	0.16	1.41	0.12	1.74	0.23	1.53	0.17
256 Tx	LoS	1.38	0.36	1.49	0.12	1.77	0.33	1.54	0.25
	NLoS	1.43	0.38	1.45	0.14	1.66	0.36	1.53	0.37
512 Tx	LoS	1.39	0.39	1.47	0.12	1.72	0.19	1.51	0.32
	NLoS	1.47	0.14	1.49	0.10	1.70	0.19	1.61	0.18
3GPP InH-Office [18]	LoS	1.60	0.18	—	—	1.62	0.22	1.22	0.23
	NLoS	1.62	0.25	—	—	1.77	0.16	1.26	0.67

NLoS environment, there is no more signal reflected from the back and the measured results become smaller than the model parameters. The ESA is larger than that in the 3GPP model also due to the difference in the measurement scenario.

The differences from the 3GPP model suggest that the impact of environments should be taken into account when using standard modeling.

C. Channel Capacity

Fig. 7 shows the variation in channel capacity as the number of transmitting antenna elements is increased from 32 to 512. It can be seen that the growth rate of channel capacity decreases as the number of transmitting antenna elements is sequentially doubled, from 51.8% to 13.3% for LoS and from 53.1% to 12.1% for NLoS. Channel capacity under i.i.d. channel does not grow significantly when the number of transmitting antenna elements is larger than 64. This is because there are only 56 antenna elements at the receiver side and the capacity tends to be saturated for transmitting antenna elements larger than this number.

In addition, there is a relatively significant difference between the channel capacity under the corridor scenario and that under the i.i.d. channel. The channel capacity in the LoS and NLoS environment reaches a maximum of 73.4% and 81.6% of the i.i.d. channel capacity, respectively. This is because the space of the corridor scenario is relatively closed and the spatial freedom of the MPCs is limited. The research in [20] finds that XL-MIMO was able to perform close to the i.i.d. channel performance in open spaces where scattering is relatively abundant.

IV. Conclusion

In this paper, we measure and analyze the PDP, delay spread, angular spread, and channel capacity of XL-MIMO in a corridor scenario concerning the impact of the number

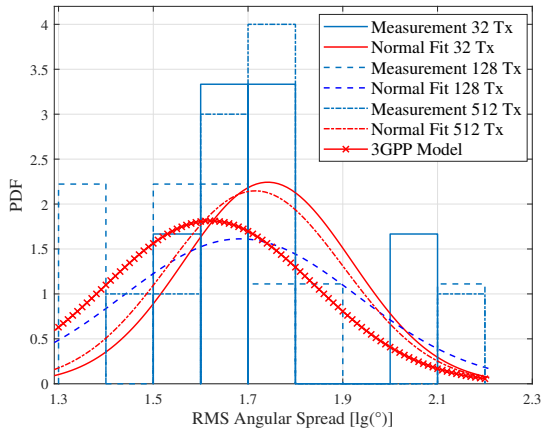

(a)

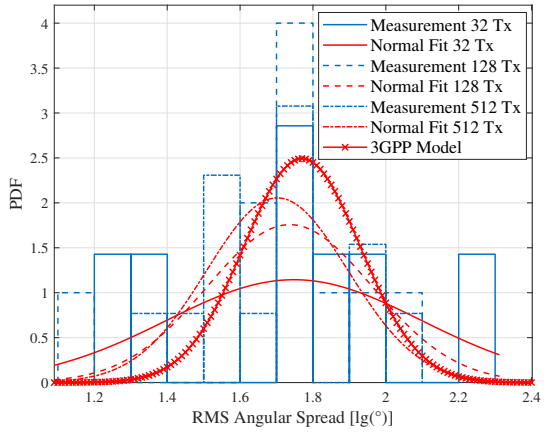

(b)

Fig. 6. ASA comparison of various numbers of TX elements and 3GPP model. (a) LoS. (b) NLoS.

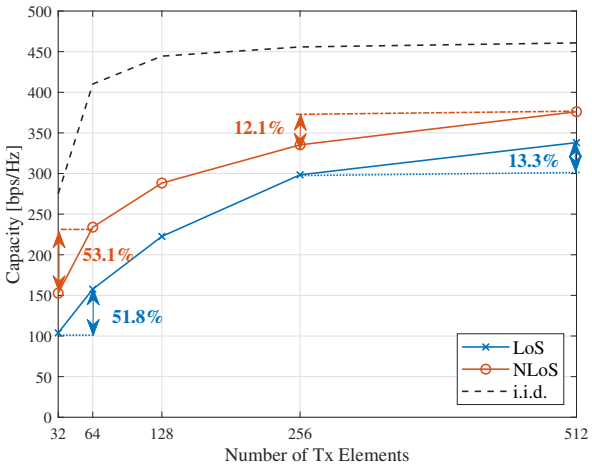

Fig. 7. Channel capacity for various number of elements, SNR=25dB.

of antenna elements and the environment. The delay spread and angular spread are not much affected by the number of antenna elements. So in this scenario, the effect of spatial non-stationarity does not need to be considered specifically when the distance between the receiver and transmitter is in the far-field range. The channel characteristics have a statistically significant difference from the 3GPP New Radio (NR) model TR 38.901. This is because the structure of the corridor has a limit to the MPCs. So the effect of the environment on channel characteristics needs to be taken into account. In terms of channel capacity, the narrow structure of the corridor limits the performance of XL-MIMO compared to i.i.d. channels. Therefore, it is not cost-effective to centrally deploy such an XL-MIMO in this kind of closed environment.

ACKNOWLEDGMENT

This research is supported in part by the National Natural Science Foundation of China (62201086, 62101069, 92167202), the National Science Fund for Distinguished Young Scholars (61925102), the Beijing University of Posts and Telecommunications-China Mobile Research Institute Joint Innovation Center, and ZTE Industry-University-Institute Cooperation Funds.

REFERENCES

[1] J. Zhang, J. Lin, P. Tang, et al., "Channel Measurement, Modeling, and Simulation for 6G: A Survey and Tutorial," *arXiv preprint arXiv: 2305.16616*, 2023.

[2] X. Lin, "An Overview of 5G Advanced Evolution in 3GPP Release 18," *IEEE Communications Standards Magazine.*, vol. 6, no. 3, pp. 77-83, Sep. 2022.

[3] J. Zhang, P. Tang, L. Yu, et al., "Channel Measurements and Models for 6G: Current Status and Future Outlook," *Frontiers of Information Technology & Electronic Engineering.*, vol. 21, no. 1, pp. 39-61, Mar. 2020.

[4] F. Rusek, D. Persson, B. K. Lau, et al., "Scaling Up MIMO: Opportunities and Challenges with Very Large Arrays," *IEEE Signal Processing Magazine.*, vol. 30, no. 1, pp. 40-60, Jan. 2013.

[5] Y. Huang, J. Zhang, J. Zhang, "Building Wireless Performance Evaluation of Channel Hardening for Massive MIMO System," *IEEE Communications Letters.*, vol. 27, no. 7, pp. 1874-1878, July 2023.

[6] X. Gao, F. Tufvesson, O. Edfors, et al., "Measured Propagation Characteristics for Very-large MIMO at 2.6 GHz," in *2012 Conference Record of the Forty Sixth Asilomar Conference on Signals, Systems and Computers (ASILOMAR).*, 2012, pp. 295–299.

[7] C. Xu, J. Zhang, Q. Zheng, et al., "Measurement-based Delay Spread Analysis of Wideband Massive MIMO System at 3.5 GHz," in *IEEE International Conference on Computational Electromagnetics.*, Apr. 2017, pp. 246-248.

[8] J. Zhang, Y. Zhang, Y. Yu, et al., "3-D MIMO: How Much Does It Meet Our Expectations Observed from Channel Mmeasurements?," *IEEE Journal on Selected Areas in Communications.*, vol. 35, no. 8, pp. 1887-1903, Aug. 2017.

[9] V. Sathya, S. M. Kala, M. I. Rochman, et al., "Standardization Advances for Cellular and Wi-Fi Coexistence in the Unlicensed 5 and 6 GHz Bands," *GetMobile: Mobile Computing and Communications.*, vol. 24, no. 1, pp. 5–15, 2020.

[10] S. Kang, M. Mezzavilla, S. Rangan, et al., "Cellular Wireless Networks in the Upper Mid-Band," *arXiv preprint arXiv: 2309.03038*, 2023.

[11] J. E. Smee, "10 Innovation Areas for 5G Advanced and Beyond [video]," Available: https://www.qualcomm.com/news/onq/2022/02/10-innovation-areas-5g-advanced-and-beyond., Feb. 2022.

[12] Samsung, "6G Spectrum: Expanding the Frontier," Available: https://cdn.codeground.org/nsr/downloads/researchareas/2022May 6G Spectrum.pdf, May. 2022.

[13] N. Li, C. Guo, D. Wang, "Considerations on 6 GHz Spectrum for 5G-Advanced and 6G," *IEEE Communications Standards Magazine.*, vol. 5, no. 3, pp. 5-7, Sep. 2021.

[14] ITU, "World Radiocommunication Conference 2023 (WRC-23)," Available: https://www.itu.int/dms_pub/itu-r/opb/act/R-ACT-WRC.15-2023-PDF-E.pdf, Dec. 2023.

[15] H. Miao, J. Zhang, P. Tang, et al., "Sub-6 GHz to mmWave for 5G-Advanced and Beyond: Channel Measurements, Characteristics and Impact on System Performance," *IEEE Journal on Selected Areas in Communications.*, vol. 41, no. 6, pp. 1945–1960, Jun. 2023.

[16] H. Yu, J. Zhang, Q. Zheng, et al., "The Rationality Analysis of Massive MIMO virtual Measurement at 3.5 GHz," in *2016 IEEE/CIC International Conference on Communications in China (ICCC Workshops).*, Aug. 2016, pp. 1-5.

[17] A. Paulraj, R. Nabar, D. Gore, "Introduction to Space-Time Wireless Communications," *Cambridge University Press.*, 2003.

[18] 3GPP, "Study on Channel Model for Frequencies from 0.5 to 100 GHz (Release 15)," *3GPP TR 38.901, Technical Report.*, Dec. 2017.

[19] J. Zhang, Z. Zheng, Y. Zhang, et al., "3D MIMO for 5G NR: Several Observations from 32 to Massive 256 Antennas Based on Channel Measurement," *IEEE Communications Magazine.*, vol. 56, no. 3, pp. 62-70, March 2018.

[20] X. Gao, O. Edfors, F. Rusek, et al., "Massive MIMO Performance Evaluation Based on Measured Propagation Data," *IEEE Transactions on Wireless Communications.*, vol. 14, no. 7, pp. 3899-3911, Jul. 2015.